IEEE Access
Multidisciplinary ⋮ Rapid Review ⋮ Open Access Journal

Received September 10, 2020, accepted September 20, 2020, date of publication September 23, 2020,
date of current version October 21, 2020.

Digital Object Identifier 10.1109/ACCESS.2020.3026054

Magnitude-Reshaping Strategy for Harmonic Suppression of VSG-Based Inverter Under Weak Grid

WEN YANG[1], MINGYU WANG[1], SADDAM AZIZ[2], (Member, IEEE), AND ALI YOUSAF KHARAL[3], (Member, IEEE)

[1]School of Electrical Engineering, Chongqing University, Chongqing 400044, China
[2]College of Mechatronics and Control Engineering, Shenzhen University, Shenzhen 518060, China
[3]National University of Sciences and Technology, Islamabad 44000, Pakistan

Corresponding author: Wen Yang (yangwen_cqu@163.com)

ABSTRACT Driven by inertial demand from the grid, the virtual synchronous generators (VSGs) are widely utilized in distributed generation systems. However, harmonic sources in the distributed generation systems with high grid impedance will cause grid voltage distortion. Distorted voltage greatly affects the power quality of VSG. Moreover, it is difficult to suppress different types of harmonics (such as sub-synchronous harmonics and non-integer high-frequency harmonics) by one conventional solution in VSG-based grid-connected system. To solve the problem, this paper proposes a magnitude-reshaping strategy to increase the output impedance in all harmonic-frequency-bands, thereby suppressing the harmonics. The magnitude-reshaping strategy consists of a notch filter and harmonic regulator. The notch filter extracts harmonic components of grid current, whereas the harmonic regulator increases the equivalent harmonic impedance. The equivalent harmonic circuit of reshaped VSG-based system is equivalent to open circuit. Therefore, the power quality of grid-connected current can be guaranteed. To analyze the performance of the magnitude-reshaping method, frequency-coupling impedance model of VSG is established. Furthermore, Comparing with the conventional harmonic suppression methods, the frequency response characteristics of the equivalent harmonic impedance are analyzed. Finally, the effectiveness of proposed control strategy is validated by experiment results.

INDEX TERMS Virtual synchronous generator, weak grid, magnitude-reshaping, harmonic suppression, frequency-coupling impedance model.

I. INTRODUCTION

With the shortage of fossil fuels and the aggravation of environmental pollution, renewable energy sources (RESs) have developed rapidly. However, the large-scale integration of RESs coupled to the grid reduces the inertia of the power system, and causes frequency and voltage changes and even leads to system instability [1]–[3]. To solve the problem of inertia shortage and frequency fluctuation, the virtual synchronous generator (VSG) control strategy for grid-connected inverter is proposed in [4]. The VSG strategy imitate the primary power regulation and primary frequency regulation characteristics of the synchronous generator to provide inertial support for the grid. With the excellent control performance, VSG control strategy is widely used in wind power generation, RESs interface in microgrid and VSC-HVDC [5], [6]. However, most of the VSG-based RESs are distributed in remote locations such as mountainous areas, islands and rural areas that are far away from cities. Thus, they are weakly connected to the grid with high impedance, which are prone to oscillations or interactions between VSG and the grid [7]. Furthermore, the grid voltage is distorted by harmonic sources in weak grid, which seriously affects the power quality of VSG.

In order to damp the current harmonics, harmonic impedance of inverter should be reshaped. Impedance reshaping methods can be realized by using passive methods [8], [9], external active methods [10]–[13], and internal active methods [14]–[21]. In the passive methods, a passive filter [8] increases the resistance in the filter of each inverter. This method is cheap and simple in design, but causes additional power losses. The performance of passive methods

The associate editor coordinating the review of this manuscript and approving it for publication was Zhilei Yao.

is severely affected by grid impedance. Compared with the performance of the passive method, the active method has a faster response and dynamic harmonic suppression capability [10]. The external active method suppresses resonance by adding external circuits and control algorithms, of which the active power filter (APF) is the most commonly used method. In [11], a global active damper method to virtualize the harmonic resistance to increase the stability of the system is proposed. Research [12] proposes another active damper method by using a low-power inverter with an LC series filter. In [13], high-pass filters are adopted for resistive active filters (R-APF) to extract harmonic components, furthermore, the product of the harmonic components and gain coefficient are fed back to the control system to achieve damping characteristics. External active methods require additional circuits and sensors. Moreover, the installation location of the external device is unchangeable.

Internal active dampers for harmonic suppression are cost effective than the external active damper. It achieves harmonic suppression by optimizing control parameters or modifying control algorithms [14]–[21]. Compared with the external active damping strategy, the optimized control algorithm is easy to operate with no power loss [15]. In [16], a phase-reshaping strategy aimed at changing the admittance phase of the inverter is proposed. However, the inverter grid-connected system as a multi-time scale system has complex phase characteristics in various frequency bands [17]. Therefore, the phase reconfiguration strategy is relatively complicated in practical applications. In [19], a control strategy including PCC voltage feedforward and grid-connected current feedback is proposed to suppress system instability and grid background harmonic disturbance. However, this method requires too many feedback parameters and is not effective in suppressing non-integer-order voltage harmonics at PCC. The same problem exists in [20], the effectiveness of harmonic suppression algorithm depends on the accuracy of the grid impedance measurement. It is difficult to suppress harmonic in different frequency bands by using conventional methods.

The harmonic suppression by resonance controller to mitigate different-order harmonics have been widely proposed in previous work. However, the working environment of a weak grid is very complicated. The background harmonics of weak grid includes integer-order harmonic, non-integer-order high-frequency harmonic and sub-synchronous oscillation. The mechanisms of the above-mentioned harmonics are completely different, and their resonance frequencies not fixed. Therefore, traditional resonance controllers cannot solve the latter two harmonic problems.

The notch-filter based method was initially implemented in [21], where genetic algorithms have been adopted to fine-tune the notch filter. Additionally, in [22], a thorough analysis of notch-filter based active damping was presented. In [23] a self-commissioning technique was proposed, which can online estimate the resonance frequency, enabling that the notch filter can be retuned accordingly. Reference [24] proposed an active damping method based on cascaded notch filter to ensure the system stability. Reference [25] used notch filter to extract the harmonic component of grid-connected current, and increase the output impedance of the inverter in high-frequency band, so as to suppress oscillation. However, the traditional notch filter-based harmonic suppression methods have not considered the local harmonic sources. In the system with local harmonic source, the quality of VSG current can be improved perfectly by notch filter-based harmonic suppression methods. However, the grid-connected current and PCC voltage are distorted. From the perspective of the grid, the power quality is substandard. Therefore the harmonics caused by VSG in parallel with different types of local harmonic sources should to be solved urgently.

Another problem to be addressed is the reshaping effect evaluation of VSG impedance. The small-signal model of VSG is established in [26], [27], in which the dynamic performance of VSG is analyzed. However, the impedance coupling is ignored. The output impedance of the VSG is coupled strongly between the frequency f_s and its complementary frequency $f_c = 2f_1 - f_s$ in low-frequency band [28]. The impedance-reshaping method may increase the coupling degree of the impedance, thus affecting the stability assessment of grid-connected system. However, most of the previous research on the modeling and analysis of VSG have focused on high-frequency dynamics [29], [30] while ignoring the effects of impedance coupling. Therefore, it is necessary to analyze the influence of the impedance shaping method on the coupling impedance of the inverter. Moreover, the equivalent harmonic impedance of the VSG-based grid-connected system needs to be established for analyzing the effect of the impedance reshaping.

The main contribution of this research is to handle these harmonic issues by one solution. Magnitude-reshaping method is proposed in this paper to improve the power quality and stability of the VSG-based grid-connected system.

The proposed method increases the VSG harmonic impedance significantly, thus the equivalent harmonic circuit of grid-connected system is equivalent to open circuit that drives the harmonic current to approach zero. For further study, the frequency-coupling impedance model of VSG is established analyzing the effects of impedance-reshaping.

The rest of the paper is organized as follows. In Section II, power quality issue of the VSG is analysed. The magnitude-reshaping strategy for harmonic suppression is proposed in Section III. Reshaping effects of proposed magnitude-reshaping strategy are described based on the frequency-coupling impedance model in Section IV. Section V compares the harmonic suppression effects with different harmonic suppression methods with three different harmonic sources connected to PCC, which validates the effectiveness of the proposed method. Finally, Section VI concludes this paper.

II. GRID-CONNECTED CURRENT DISTORTION ISSUE OF VSG IN WEAK GRID

Different types of local sources of harmonics exist in the three-phase weak grid. When both the VSG and the local

harmonic source are connected to the PCC, the power quality of the grid deteriorates.

This paper studies three different types of harmonics (integer-order harmonic, non-integer-order high-frequency harmonic and sub-synchronous oscillation) in the system.

i) Sub-synchronous oscillation: it is caused by shaft vibration of synchronous generator, and its oscillation frequency is generally less than 50 Hz;

ii) integer-order harmonic: it is caused by nonlinear load;

iii) non-integer-order high-frequency harmonic: it is caused by the grid-source oscillations, which leads to critical stability or instability of the system.

The mechanisms of these harmonics are different. The impacts of the above-mentioned local harmonic sources on power quality are explained as follows.

A. NON-INTEGER-ORDER HARMONIC: DISTRIBUTED GENERATION

Topology of VSG in parallel with three-phase distributed generation system is shown in Figure 1(a). The small signal model of the grid-connected system is established by harmonic linearization method, as shown in Figure 1(b). The harmonic-domain circuit of distributed source is equivalent to a current-controlled source in parallel with the output impedance $Z_{\mathrm{DGh}}(s)$.

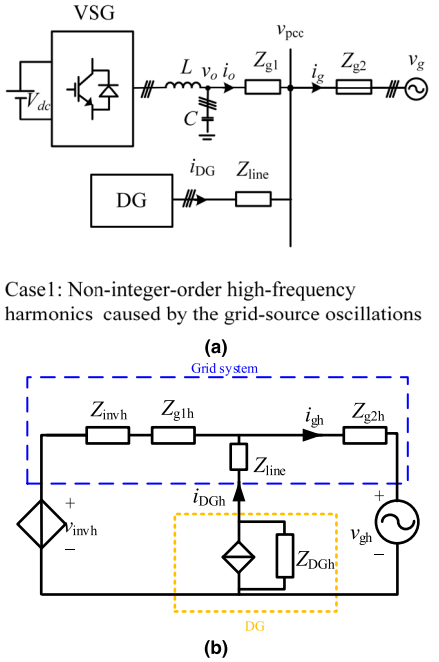

FIGURE 1. Topology and the small signal model VSG-based grid-connected system in parallel with distributed generation.

While the distributed source DG operates in the weak grid (with large grid impedance Z_{g2}), the grid-connected system may be critical oscillation or unstable. The stability of the system depends on the short circuit ratio (*SCR*) from the perspective of DG.

$$SCR = \frac{v_{DGN}^2}{P_{DG} Z_{gs}} \tag{1}$$

where Z_{gs} is the equivalent impedance in the blue dotted area.

When the interactive oscillation occurs in interactive system, the i_{DGh} contains non-integer-order harmonic components. The i_{gh} can be expressed as:

$$\begin{aligned} i_{\mathrm{gh}}(s) = & \frac{v_{\mathrm{invh}}(s)}{Z_{\mathrm{invh}}(s) + Z_{\mathrm{g1h}}(s) + Z_{\mathrm{g2h}}(s) \,//\, (Z_{\mathrm{lineh}} + Z_{\mathrm{DGh}})} \\ & - \frac{v_{\mathrm{gh}}(s)}{Z_{\mathrm{g2h}}(s) + \left(Z_{\mathrm{invh}}(s) + Z_{\mathrm{g1h}}(s)\right) \,//\, (Z_{\mathrm{lineh}} + Z_{\mathrm{DGh}})} \\ & + i_{\mathrm{DGh}}(s) \frac{Z_{\mathrm{invh}}(s) + Z_{\mathrm{g1h}}(s)}{Z_{\mathrm{g2h}}(s) + Z_{\mathrm{invh}}(s) + Z_{\mathrm{g1h}}(s)} \end{aligned} \tag{2}$$

It is assumed that the harmonic components of v_{g} and v_{inv} are small. Then the harmonic component of i_{g} can be expressed as

$$i_{\mathrm{gh}}(s) \approx i_{\mathrm{DGh}}(s) \frac{Z_{\mathrm{invh}}(s) + Z_{\mathrm{g1h}}(s)}{Z_{\mathrm{g2h}}(s) + Z_{\mathrm{invh}}(s) + Z_{\mathrm{g1h}}(s)} \tag{3}$$

B. INTEGER-ORDER HARMONIC: NONLINEAR LOAD

Topology of VSG-based grid-connected system with three-phase local nonlinear load is shown in Figure 2(a). The small signal model of three-phase the grid-connected system is established by harmonic linearization method, as shown in Figure 2(b). The VSG is equivalent to a voltage source in series with a output impedance Z_{inv}(s). The harmonic-domain circuit of nonlinear load is equivalent to a harmonic current source.

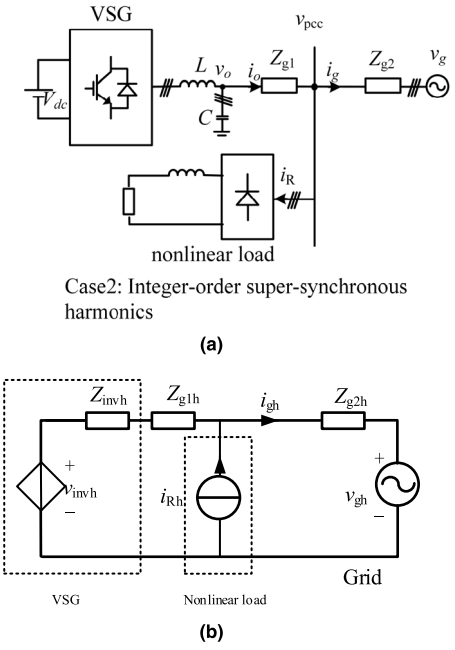

FIGURE 2. Topology and the small signal model of VSG-based grid-connected system with nonlinear load.

The harmonic component of i_g is mainly caused by the switching action of local nonlinear load. The nonlinear loads is equivalent to integer-order (such as 5^{th}, 7^{th}, 11^{th} and 13^{th}) harmonic source in parallel with impedance. The grid- connected harmonic current i_{gh} can be expressed as:

$$i_{gh}(s) = \frac{v_{invh}(s) - v_{gh}(s)}{Z_{inv}(s) + Z_{g1}(s) + Z_{g2}(s)} + \frac{i_{Rh}(s)\left(Z_{g2h}(s) // \left(Z_{invh}(s) + Z_{g1h}(s)\right)\right)}{Z_{g2h}(s)} \quad (4)$$

It is assumed that the harmonic components of v_g and v_{inv} are small. Then the harmonic component of i_g can be expressed as:

$$i_{gh}(s) \approx \frac{i_{Rh}(s)\left(Z_{g2h}(s) // \left(Z_{invh}(s) + Z_{g1h}(s)\right)\right)}{Z_{g2h}(s)} = \frac{i_{Rh}(s)}{1 + Z_{g2h}(s)/\left[\left(Z_{g1h}(s) + Z_{invh}(s)\right)\right]} \quad (5)$$

C. HARMONIC SOURCE: SYNCHRONOUS GENERATOR

Topology of VSG-based grid-connected system with synchronous generator is shown in Figure 3(a). The small signal model of the three-phase grid-connected system is established by harmonic linearization method, as shown in Figure 3(b). The harmonic-domain circuit of synchronous generator is equivalent to the voltage source.

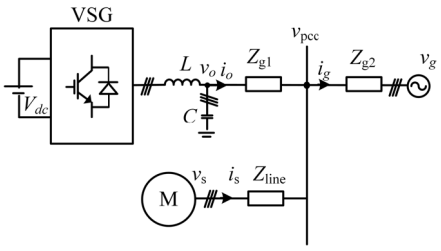

Case3：Sub-synchronous oscillation caused by shaft vibrations of synchronous generator

(a)

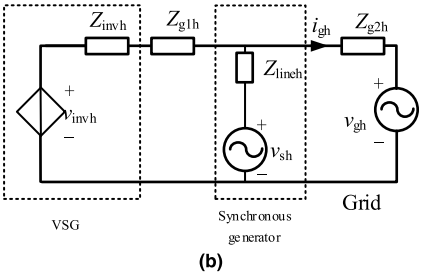

(b)

FIGURE 3. Topology and the small signal model of VSG-based grid-connected system with synchronous generator.

When shaft oscillation occurs in the system, the voltage of synchronous generator v_{sh} contains sub-synchronous harmonic. In this case, the grid-connected current i_{gh} can be expressed as:

$$i_{gh}(s) = \frac{v_{invh}(s)\left(\frac{Z_{lineh}}{Z_{lineh}+Z_{g2h}(s)}\right)}{Z_{invh}(s) + Z_{g1h}(s) + Z_{g2h}(s) // Z_{lineh}} - \frac{v_{gh}(s)}{Z_{g2h}(s) + \left(Z_{invh}(s) + Z_{g1h}(s)\right) // Z_{lineh}} + \frac{v_{sh}(s)\left(\frac{Z_{invh}(s)+Z_{g1h}(s)}{Z_{invh}(s)+Z_{g1h}(s)+Z_{g2h}(s)}\right)}{Z_{lineh} + Z_{g2h}(s) // \left(Z_{invh}(s) + Z_{g1h}(s)\right)} \quad (6)$$

It is assumed that the harmonic components of v_g and v_{inv} are small. Then the harmonic component of i_g can be expressed as:

$$i_{gh}(s) \approx \frac{v_{sh}(s)\left(\frac{Z_{invh}(s)+Z_{g1h}(s)}{Z_{invh}(s)+Z_{g1h}(s)+Z_{g2h}(s)}\right)}{Z_{line} + Z_{g2h}(s) // \left(Z_{invh}(s) + Z_{g1h}(s)\right)} \quad (7)$$

The above-mentioned harmonics may lead to a serious distorted harmonic grid current $i_{gh}(s)$. If the sum of harmonic impedance of inverter and power grid is too small, it leads to the total harmonic distortion (THD) of grid current larger than the grid-connected standard (<5%). Then, the adaptability that VSG cannot be guaranteed. Moreover, if the sum of harmonic impedances of the inverter and the grid has negative real part, the system will have poles in the left plane, which leads the grid-connected system to instability.

The control target of this paper is to suppress the grid-connected harmonic current i_{gh}. The harmonic current in the grid is absorbed by the VSG, so that the local harmonic source will not bring harmonic problems to the grid. Therefore, the VSG should be designed and controlled properly to improve the power quality.

III. MAGNITUDE-RESHAPING STRATEGY FOR HARMONIC SUPPRESSION IN VSG

A. SHORTAGE OF PREVIOUS HARMONIC SUPPRESSION SCHEME FOR VSG

Voltage feedback strategy is the most widely used for harmonic suppression. It is done by feeding back the PCC voltage into the control system to track the PCC harmonic voltage, as shown in Figure 4(a). Harmonic regulator uses the proportional control to increase harmonic impedance. However, it is also hard to address the power quality of VSG at high-frequency band.

Impedance-based harmonic suppression method is another solution to solve the problem [17]. It is realized by feedback of the potential difference of additional inductance Z_{sh} into the control system to track harmonic voltages of v_{pcc} and v_{sh}, as shown in Figure 4(b). Harmonic regulator usually adopts the multi-resonant control to increase harmonic impedance, which is expressed as [17]:

$$G_h(s) = \sum_{i=5,7,11,13,17,19} \frac{2\omega_c s + \omega_c^2}{s^2 + 2\omega_c s + (i\omega_n)^2 + \omega_c^2} \quad (8)$$

where i is the number of major harmonics, and ω_n is the fundamental angular frequency. Similarly, this method cannot suppress high-frequency harmonics perfectly.

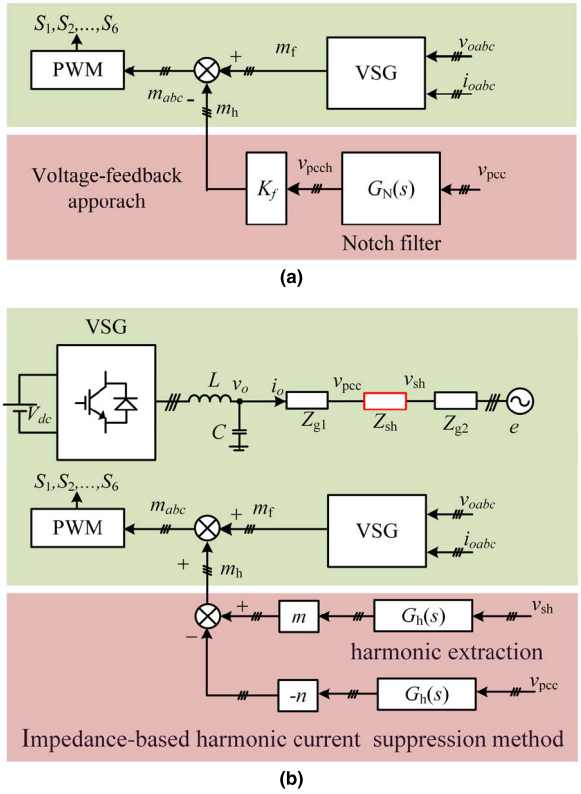

FIGURE 4. Topology of harmonic suppression strategy: (a) Voltage feedback strategy. (b) Impedance-based harmonic suppression method.

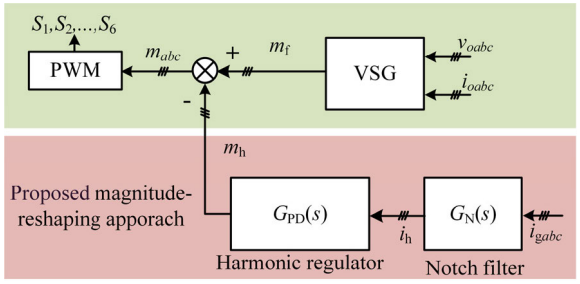

FIGURE 5. Proposed magnitude-reshaping strategy.

B. PROPOSED MAGNITUDE-RESHAPING METHOD FOR VSG

To address the power quality issue in VSG-based grid-connected system, the impedance-based magnitude-reshaping method is proposed as shown in Figure 5. The output impedance of VSG is reshaped by feedback variables i_{gabc}. i_h represents the harmonic component i_{oabc}, which is obtained through notch filter $G_N(s)$. Then the harmonic regulator $G_{PD}(s)$ improves the output impedance of the inverter in the harmonic frequency region and generates the harmonic voltage reference m_h.

The harmonic voltage reference of VSG (m_h) is expressed as:

$$m_h = G_{MR}(s)\, i_g = G_{PD}(s)\, G_N(s)\, (i_o + i_R) \tag{9}$$

The notch filter is adopted to obtain the harmonic currents of the inverter. The expression of $G_h(s)$ are given as:

$$G_N(s) = \frac{s^2 + \omega_n^2}{s^2 + 2\omega_c s + \omega_n^2} \tag{10}$$

where ω_c is the cutoff frequency with value of 4π rad/s, which means that the impedance reshaping strategy has no effect on the frequency band in the range of [48 Hz, 50 Hz], and will not interfere with the fundamental component of the VSG output current. On basis of (10), it is derived that $|G_N(f_h)| = 1$.

The harmonic regulator $G_{PD}(s)G_{PD}(s)$ is given as:

$$G_{PD}(s) = K_p + K_d s \tag{11}$$

where K_d is the differential coefficient used for increasing high-frequency harmonic impedance and K_p is proportional coefficient aimed to increase harmonic impedance in the sub-synchronous frequency region. The Bode plot of $G_{MR}(s)$ is shown in Figure 6.

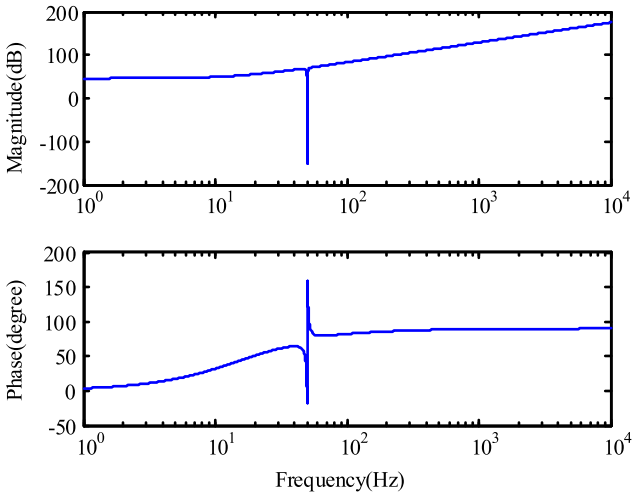

FIGURE 6. The Bode plot of magnitude-reshaping regulator $G_{MR}(s)$.

C. HARMONIC SUPPRESSION MECHANISM OF MAGNITUDE-RESHAPING METHOD

Before introducing magnitude-reshaping strategy, the modulation signal m_{abc} can be obtained in the control system by sampling the output voltages and currents as:

$$\begin{bmatrix} m_a \\ m_b \\ m_c \end{bmatrix} = G_{mi}(s) \begin{bmatrix} i_{oa} \\ i_{ob} \\ i_{oc} \end{bmatrix} + G_{mv}(s) \begin{bmatrix} v_{oa} \\ v_{ob} \\ v_{oc} \end{bmatrix} \tag{12}$$

where $G_{mi}(s)$ and $G_{mv}(s)$ are the transfer functions associated with VSG control system derived in Section IV.

The state space equation of the main circuit are given as:

$$sL \begin{bmatrix} i_{oa} \\ i_{ob} \\ i_{oc} \end{bmatrix} = K_m V_{dc} \begin{bmatrix} m_a \\ m_b \\ m_c \end{bmatrix} - \left(1 + s^2 LC\right) \begin{bmatrix} v_{oa} \\ v_{ob} \\ v_{oc} \end{bmatrix} \tag{13}$$

where K_m is the modulator gain.

Substituting (12) in (13), the output impedance of the inverter can be obtained as:

$$Z_{\text{inv}}(s) = -\frac{v_{oa}}{i_{oa}} = \frac{sL - K_m V_{\text{dc}} G_{mi}(s)}{1 + s^2 LC - K_m V_{\text{dc}} G_{mv}(s)} \tag{14}$$

After introducing magnitude-reshaping strategy, the modulation signal m_{abc} consists of harmonic voltage value m_{h} and fundamental voltage m_f, as seen from Figure 5.

$$\begin{bmatrix} m_a \\ m_b \\ m_c \end{bmatrix} = G_{mi}(s) \begin{bmatrix} i_{oa} \\ i_{ob} \\ i_{oc} \end{bmatrix} + G_{mv}(s) \begin{bmatrix} v_{oa} \\ v_{ob} \\ v_{oc} \end{bmatrix} - G_{\text{MR}}(s) \begin{bmatrix} i_{ga} \\ i_{gb} \\ i_{gc} \end{bmatrix} \tag{15}$$

where

$$\begin{bmatrix} i_{oa} \\ i_{ob} \\ i_{oc} \end{bmatrix} = \begin{bmatrix} i_{ga} \\ i_{gb} \\ i_{gc} \end{bmatrix} - \begin{bmatrix} i_{\text{R}a} \\ i_{\text{R}b} \\ i_{\text{R}c} \end{bmatrix},$$
$$\begin{bmatrix} v_{oa} \\ v_{ob} \\ v_{oc} \end{bmatrix} = \begin{bmatrix} v_{\text{pcc}a} \\ v_{\text{pcc}b} \\ v_{\text{pcc}c} \end{bmatrix} + Z_{\text{g1}}(s) \begin{bmatrix} i_{oa} \\ i_{ob} \\ i_{oc} \end{bmatrix}$$

Ignoring the disturbance signal i_{R} in the transfer function. Substituting (15) in (13), the equivalent impedance view from PCC to VSG can be derived as:

$$\begin{aligned} Z_{\text{eq}}(s) &= -\frac{v_{pcca}}{i_{ga}} = \frac{sL - K_m V_{\text{dc}}(G_{mi}(s) - G_{\text{MR}}(s))}{1 + s^2 LC - K_m V_{\text{dc}} G_{mv}(s)} + Z_{\text{g1}}(s) \\ &= Z_{\text{inv}}(s) + \frac{K_m V_{\text{dc}} G_{\text{MR}}(s)}{1 + s^2 LC - K_m V_{\text{dc}} G_{mv}(s)} + Z_{\text{g1}}(s) \\ &= Z_{\text{inv}}(s) + Z_{\text{vir}}(s) + Z_{\text{g1}}(s) \end{aligned} \tag{16}$$

In order to ensure the power quality of PCC voltage and grid current, the reshaped impedance of the VSG should be close to infinity in the harmonic band. The fundamental impedance and harmonic virtual impedance are derived as:

$$Z_{\text{vir}}(s)|_{s=f_1} = \lim_{s \to f_1} \frac{K_m V_{\text{dc}}(K_d s + K_p)}{1 + s^2 LC + \infty} = 0 \tag{17}$$

$$\lim_{s \to 0} Z_{\text{vir}}(s) \approx \lim_{s \to 0} \frac{K_m V_{\text{dc}} K_p}{1 + s^2 LC - K_m V_{\text{dc}} G_{mv}(s)} = K_m V_{\text{dc}} K_p \tag{18}$$

$$\lim_{s \to f_c} Z_{\text{vir}}(s) \approx \lim_{s \to f_c} \frac{K_m V_{\text{dc}} K_d s}{1 + s^2 LC - K_m V_{\text{dc}} G_{mv}(s)} = K_m V_{\text{dc}} K_d s \tag{19}$$

where f_{c} is the switch frequency. From (17) to (19), it is noted that the virtual impedance magnitude in the low-frequency band is mainly determined by K_{p}, and the impedance magnitude in the high-frequency band is determined by differential coefficient K_{d}.

The following three cases are used to discuss the harmonic suppression mechanism of virtual impedance Z_{vir}.

Equivalent circuit of reshaped VSG-based grid-connected system with nonlinear load is shown in Figure 7. It is assumed that the harmonic components of v_{g} and v_{inv}

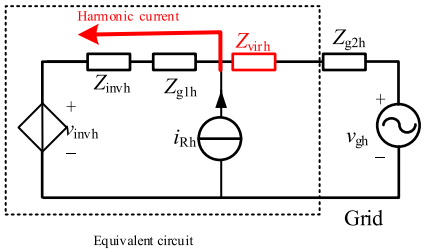

FIGURE 7. Equivalent circuit of reshaped VSG-based grid-connected system with nonlinear load.

are small. Then the harmonic components of i_{g} can be expressed as

$$\begin{aligned} i_{\text{gh}}(s) &\approx \frac{i_{\text{Rh}}(s)\left(\left(Z_{\text{g2}}(s) + Z_{\text{virh}}(s)\right) // \left(Z_{\text{invh}}(s) + Z_{\text{g1h}}(s)\right)\right)}{\left(Z_{\text{g2}}(s) + Z_{\text{vir}}(s)\right)} \\ &= \frac{i_{\text{Rh}}(s)}{1 + \left(Z_{\text{g2h}}(s) + Z_{\text{virh}}(s)\right) / \left[\left(Z_{\text{g1h}}(s) + Z_{\text{invh}}(s)\right)\right]} \\ &= \frac{i_{\text{Rh}}(s)}{1 + \left(Z_{\text{g2h}}(s) + Z_{\text{virh}}(s)\right) / K_1(s)} \end{aligned} \tag{20}$$

The Magnitude-reshaping method is equivalent to add a virtual impedance Z_{vir} into the system. If $|Z_{\text{g2h}} + Z_{\text{virh}}| \gg |K_1(s)|$, then the harmonic components of i_{gh} reduce.

$$v_{\text{pcch}}(s) = i_{\text{gh}}(s) Z_{\text{g2}}(s) \tag{21}$$

According to (21), the harmonic components of v_{pcc} also decrease. Most of the harmonic current flows into the VSG. Therefore, Magnitude-reshaping method improves the power quality by adding Z_{vir}.

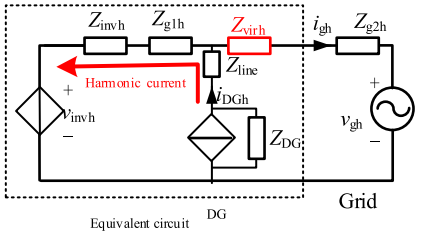

FIGURE 8. Equivalent circuit of reshaped VSG-based grid-connected system in parallel with distributed generation.

Equivalent circuit of reshaped VSG-based grid-connected system with distributed generation is shown in Figure 8. The Magnitude-reshaping method is equivalent to add a virtual impedance Z_{virh} into the system. With Magnitude-reshaping method enable, the harmonic component of i_{g} can be expressed as:

$$\begin{aligned} i_{\text{gh}}(s) &\approx i_{\text{DGh}}(s) \frac{Z_{\text{invh}}(s) + Z_{\text{g1h}}(s)}{Z_{\text{g2h}}(s) + Z_{\text{virh}}(s) + Z_{\text{invh}}(s) + Z_{\text{g1h}}(s)} \\ &= i_{\text{DGh}}(s) \frac{1}{1 + \left(Z_{\text{g2h}}(s) + Z_{\text{virh}}(s)\right) / K_2(s)} \end{aligned} \tag{22}$$

If $|Z_{\text{g2h}} + Z_{\text{virh}}| \gg |K_2(s)|$, then the harmonic components of i_{gh} sharply reduce. PCC voltage is given as:

$$v_{\text{pcc}}(s) = v_{\text{gh}}(s) + Z_{\text{g2h}}(s) i_{\text{gh}}(s) \approx v_{\text{gh}}(s) \tag{23}$$

Then from the perspective of distributed source, equivalent grid impedance Z_{gs} reduced. Z_{gs} can be derived as:

$$\begin{aligned} &Z_{gs}(s) \\ &= Z_{lineh}(s) + \left(Z_{g1h}(s) + Z_{invh}(s)\right) // \left(Z_{g2h}(s) + Z_{virh}(s)\right) \\ &\approx Z_{lineh}(s) \end{aligned} \tag{24}$$

Therefore, the SCR of system decreases. According to the impedance stability criterion, the conditions for interactive oscillation no longer exist. The stability of the grid-connected system is improved. Therefore, the magnitude of the resonance current i_{DGh} is greatly attenuated. The power quality is guaranteed.

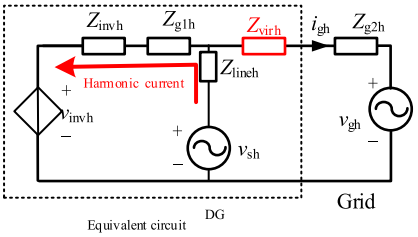

FIGURE 9. Equivalent circuit of reshaped VSG-based grid-connected system in parallel with synchronous generator.

Equivalent circuit of reshaped VSG-based grid-connected system with nonlinear load is shown in Figure 9. The magnitude-reshaping method is equivalent to add a virtual impedance Z_{vir} into the system. After adding a virtual impedance Z_{vir} into the system, the harmonic components of i_g can be expressed as:

$$\begin{aligned} &i_{gh}(s) \\ &= \frac{v_{sh}(s)\left(\frac{Z_{invh}(s)+Z_{g1h}(s)}{Z_{invh}(s)+Z_{g1h}(s)+\left(Z_{g2h}(s)+Z_{virh}(s)\right)}\right)}{Z_{lineh}(s) + \left(Z_{g2h}(s) + Z_{virh}(s)\right) // \left(Z_{invh}(s) + Z_{g1h}(s)\right)} \\ &= \frac{v_{sh}(s)}{\left(Z_{g2h}(s) + Z_{virh}(s)\right)\left(1 + Z_{lineh}(s) \big/ \left(Z_{invh}(s) + Z_{g1h}(s)\right)\right)} \\ &= v_{sh}(s)\frac{1}{\left(Z_{g2h}(s) + Z_{virh}(s)\right)\left(1 + K_3(s)\right)} \end{aligned} \tag{25}$$

If $|Z_{g2h} + Z_{virh}| \gg |1 + K_3(s)|$, then the harmonic components of i_{gh} reduce. Most of the harmonic current flows into the VSG. In this case, Magnitude-reshaping method improves the power quality.

From the perspective of impedance reshaping, the purpose of magnitude-reshaping strategy is to improve the harmonic virtual impedance and make the harmonic path of grid connected-system equivalent to open circuit, which improves the robustness of VSG against grid background harmonics.

IV. RESHAPING PERFORMANCE OF MAGNITUDE-RESHAPING STRATEGY BASED ON FREQUENCY-COUPLING IMPEDANCE MODELING

A. FREQUENCY-COUPLING IMPEDANCE MODELING FOR EQUAVILANT IMPEDANCE

In order to analyze the effects of the magnitude-reshaping strategy on the grid-connected system, a frequency-coupling

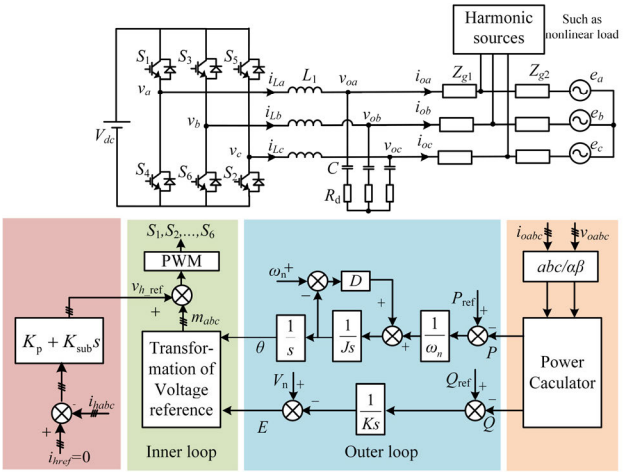

FIGURE 10. Topology and control diagram of VSG.

impedance model of VSG is established in this section. The structure and control system of VSG-based grid-connected system is shown in Figure 10. V_{dc} is DC-side voltage; v_{oa}, v_{ob}, and v_{oc} are output voltages of the inverter; i_{oa}, i_{ob} and i_{oc} are the output currents of the inverter. The L and C is the filter inductor and filter capacitor, respectively. i_g is the grid-connected current; v_g is the grid voltage; Z_g is the grid impedance. P and Q are the instantaneous output power of inverter. P_{ref} and Q_{ref} are the power references of inverter. The error signals between instantaneous output power and the power reference are sent to VSG controller to generate the amplitude E and angle θ of VSG internal voltage. Then, the modulation signal m_{abc} is generated by coordinated rotation. Finally, the gate signals of IGBT are generated in the PWM modulator.

In the time domain, the output voltage and current with small perturbations can be written as:

$$\begin{aligned} v_{oa}(t) &= V_1\cos\left(2\pi f_1 t + \theta_{v1}\right) + V_s\cos\left(2\pi f_p t + \theta_{vs}\right) \\ &\quad + V_c\cos\left(2\pi f_c t + \theta_{vc}\right) \end{aligned} \tag{26}$$

$$\begin{aligned} i_{oa}(t) &= I_1\cos\left(2\pi f_1 t + \theta_{i1}\right) + I_s\cos\left(2\pi f_p t + \theta_{is}\right) \\ &\quad + I_c\cos\left(2\pi f_c t + \theta_{ic}\right) \end{aligned} \tag{27}$$

where f_1, f_s, f_c are the fundamental frequency and the two complementary harmonic frequencies, respectively, with $f_c = 2f_1 - f_s$; V_1, V_s, and V_c are the amplitude of voltages at f_1, f_s and f_c, respectively; I_1, I_s, and I_c are the amplitudes of currents at f_1, f_s and f_c; θ_{v1}, θ_{vs} and θ_{vc} are phase angles correspond to voltages, and the current angles follow the same notation.

In the frequency domain, the phasor representations are given as [2]:

$$\dot{V}_{oa}[f] = \begin{cases} \dot{V}_1, & f = f_1 \\ \dot{V}_s, & f = \pm f_s \\ \dot{V}_c, & f = \pm f_c, \end{cases} \quad \dot{I}_{oa}[f] = \begin{cases} \dot{I}_1, & f = f_1 \\ \dot{I}_s, & f = \pm f_s \\ \dot{I}_c, & f = \pm f_c \end{cases} \tag{28}$$

where $\dot{V}$ is vector expression of V_1, $\dot{V}_1 = V_1\angle\theta_{v1}$, $\dot{V}_s = V_s\angle\theta_{vs}$, $\dot{V}_c = V_c\angle\theta_{vc}$ and output currents follow the same notation.

The instantaneous power of the inverter is given as:

$$\begin{cases} P(t) = v_{oa}i_{oa} + v_{ob}i_{ob} + v_{oc}i_{oc} \\ Q(t) = \left[\left(v_{ob} - v_{oc}\right) i_{oa} + \left(v_{oc} - v_{oa}\right) i_{ob} \right. \\ \qquad \left. + \ \left(v_{oa} - v_{ob}\right) i_{oc}\right] / \sqrt{3} \end{cases} \tag{29}$$

Substituting (28) in (29) and ignoring DC component and high-order perturbation components, the vector expressions of output power are calculated as:

$$\begin{aligned} \begin{bmatrix} \dot{P}[f] \\ \dot{Q}[f] \end{bmatrix} = +1.5 \begin{bmatrix} \dot{V}_1^* & \dot{V}_1 \\ j\dot{V}_1^* & -j\dot{V}_1 \end{bmatrix} \begin{bmatrix} \dot{I}_s \\ \dot{I}_c^* \end{bmatrix} \\ + 1.5 \begin{bmatrix} \dot{I}_1^* & \dot{I}_1 \\ -j\dot{I}_1^* & j\dot{I}_1 \end{bmatrix} \begin{bmatrix} \dot{V}_s \\ \dot{V}_c^* \end{bmatrix}, \quad f = f_p - f_1 \end{aligned} \tag{30}$$

where * denotes complex conjugation.

VSG controller imitates primary voltage regulation and frequency modulation characteristics of synchronous generator. As shown in the VSG controller structure in Figure 1, the expression of $G_P(s)$ and $G_Q(s)$ can be obtained as follows:

$$\begin{cases} G_P(s) = \dfrac{1}{s\left(Js + D\right)} \\ G_Q(s) = \dfrac{1}{Ks} \end{cases} \tag{31}$$

where J is the virtual inertia, D is the damping coefficient, and K is droop coefficient. ω_1 is the fundamental angular frequency.

The error signals of the instantaneous power and the rated power are sent to the power controller $G_P(s)$ and $G_Q(s)$.

$$\begin{cases} \dot{\theta} = G_P(s)\,\dot{P} \\ \dot{E} = G_Q(s)\,\dot{Q} \end{cases} \tag{32}$$

Neglecting second-order perturbations and substituting (30) in (32) the expression of $\hat{\theta}$ and $\hat{E}$ in the frequency-domain are derived as follows:

$$\begin{aligned} \begin{bmatrix} \dot{\theta}[f] \\ \dot{E}[f] \end{bmatrix} = \begin{bmatrix} 1.5\dot{V}_1^* G_P(s) & 1.5\dot{V}_1 G_P(s) \\ j1.5\dot{V}_1^* G_E(s) & -j1.5\dot{V}_1 G_E(s) \end{bmatrix} \begin{bmatrix} \dot{I}_s \\ \dot{I}_c^* \end{bmatrix} \\ + \begin{bmatrix} 1.5\dot{I}_1^* G_P(s) & 1.5\dot{I}_1 G_P(s) \\ -j1.5\dot{I}_1^* G_Q(s) & j1.5\dot{I}_1 G_Q(s) \end{bmatrix} \begin{bmatrix} \dot{V}_s \\ \dot{V}_c^* \end{bmatrix} \\ s = s_s - s_1, \quad f = f_s - f_1 \end{aligned} \tag{33}$$

The voltage transformation converts the voltage from the $E\theta$ polar coordinate frame to the three-phase stationary coordinate frame. The voltage modulating signal of VSG algorithm of phase A is written as follows:

$$\begin{cases} m_{\mathrm{fa}}(t) = \left(E_1 + \hat{E}\right)\cos\left(\omega_1 t + \theta_1 + \hat{\theta}\right) \\ m_{\mathrm{fb}}(t) = \left(E_1 + \hat{E}\right)\cos\left(\omega_1 t + \theta_1 - 2\pi/3 + \hat{\theta}\right) \\ m_{\mathrm{fc}}(t) = \left(E_1 + \hat{E}\right)\cos\left(\omega_1 t + \theta_1 + 2\pi/3 + \hat{\theta}\right) \end{cases} \tag{34}$$

where $\hat{E}$ and $\hat{\theta}$ are disturbances at frequency $f_p - f_1$.

Since $\hat{\theta}$ is far less than 1, it is assumed that $\cos\hat{\theta} = 1$ and $\sin\hat{\theta} = \hat{\theta}$. According to the principle of harmonic linearization, we can simplify (34) by removing the second-order and higher-order terms of the perturbation Hence, the first-order term of the voltage modulating signal of VSG algorithm can be derived as:

$$m_{\mathrm{fa}}(t) = \hat{E}\cos\left(\omega_1 t + \theta_1\right) - \hat{\theta}E_1\sin\left(\omega_1 t + \theta_1\right) \tag{35}$$

where $\cos\left(\omega_1 t + \theta_1\right)$ and $\sin\left(\omega_1 t + \theta_1\right)$ are ac signals with frequency of f_1.

In (35), the product of ac signals produces harmonics with two complementary frequencies of f_s and f_c. When system is in steady state, voltage modulating signal of VSG algorithm can be derived in the frequency-domain:

$$\begin{bmatrix} \dot{M}_{fs}[f_s] \\ \dot{M}_{fc}^*[f_c] \end{bmatrix} = \frac{1}{2}\begin{bmatrix} \dot{E}_1 & j\dot{\theta}_1 \\ \dot{E}_1^* & -j\dot{\theta}_1^* \end{bmatrix} \begin{bmatrix} \dot{\theta}_{\mathrm{ref}}[f] \\ \dot{E}_{\mathrm{ref}}[f] \end{bmatrix}, \quad f = f_s - f_1 \tag{36}$$

where $\dot{E}_1 = j2\pi f_1 L\dot{I}_1 + \dot{V}_1$ is the vector representation of $E_1\sin\left(\omega t + \theta_1\right)$; and $\dot{\theta}_1 = \dot{E}_1 / \left|\dot{E}_1\right|$.

Combining (33) and (36), the modulating signal of the VSG is derived as:

$$\begin{aligned} &\begin{bmatrix} \dot{M}_{fs}[f_s] \\ \dot{M}_{fc}^*[f_c] \end{bmatrix} \\ &= \frac{3}{4}\begin{bmatrix} \dot{E}_1\dot{V}_1^* G_P(s) - \dot{\theta}_1\dot{V}_1^* G_E(s) & \dot{E}_1\dot{V}_1 G_P(s) + \dot{\theta}_1\dot{V}_1 G_E(s) \\ \dot{E}_1^*\dot{V}_1^* G_P(s) + \dot{\theta}_1^*\dot{V}_1^* G_E(s) & \dot{E}_1^*\dot{V}_1 G_P(s) - \dot{\theta}_1^*\dot{V}_1 G_E(s) \end{bmatrix} \\ &\quad \times \begin{bmatrix} \dot{I}_s \\ \dot{I}_c^* \end{bmatrix} + \frac{3}{4} \\ &\quad \times \begin{bmatrix} \dot{E}_1\dot{I}_1^* G_P(s) + \dot{\theta}_1\dot{I}_1^* G_Q(s) & \dot{E}_1\dot{I}_1 G_P(s) - \dot{\theta}_1\dot{I}_1 G_Q(s) \\ \dot{E}_1^*\dot{I}_1^* G_P(s) - \dot{\theta}_1^*\dot{I}_1^* G_Q(s) & \dot{E}_1^*\dot{I}_1 G_P(s) + \dot{\theta}_1^*\dot{I}_1 G_Q(s) \end{bmatrix} \\ &\quad \times \begin{bmatrix} \dot{V}_s \\ \dot{V}_c^* \end{bmatrix} = \mathbf{G}_{mi}(s)\begin{bmatrix} \dot{I}_s \\ \dot{I}_c^* \end{bmatrix} + \mathbf{G}_{mv}(s)\begin{bmatrix} \dot{V}_s \\ \dot{V}_c^* \end{bmatrix}, \quad s = s_s - s_1 \end{aligned} \tag{37}$$

The current responses to the voltage perturbation can be found by the systems state space equation:

$$\begin{aligned} \begin{bmatrix} s_s L_1 & 0 \\ 0 & s_c L_1 \end{bmatrix} \begin{bmatrix} \dot{I}_s \\ \dot{I}_c^* \end{bmatrix} = K_m V_{dc} \begin{bmatrix} \dot{M}_s \\ \dot{M}_c^* \end{bmatrix} \\ - \begin{bmatrix} 1 + s_s^2 L_1 C & 0 \\ 0 & 1 + s_c^2 L_1 C \end{bmatrix} \begin{bmatrix} \dot{V}_s \\ \dot{V}_c^* \end{bmatrix} \end{aligned} \tag{38}$$

Combining (37) and (38), the current-voltage vector relation of the VSG is derived as:

$$\begin{aligned} \begin{bmatrix} \dot{V}_s \\ \dot{V}_c^* \end{bmatrix} &= \left(K_m V_{dc}\mathbf{G}_{mv}(s_s - s_1) - \begin{bmatrix} 1 + s_s^2 L_1 C & 0 \\ 0 & 1 + s_c^2 L_1 C \end{bmatrix}\right) \backslash \\ &\quad \left(\begin{bmatrix} s_s L_1 & 0 \\ 0 & s_c L_1 \end{bmatrix} - K_m V_{dc}\mathbf{G}_{mi}(s_s - s_1)\right) \begin{bmatrix} \dot{I}_s \\ \dot{I}_c^* \end{bmatrix} \\ &= \begin{bmatrix} Z_{ss}(s_s) & Z_{sc}(s_c) \\ Z_{cs}(s_s) & Z_{cc}(s_c) \end{bmatrix} \begin{bmatrix} -\dot{I}_s \\ -\dot{I}_c^* \end{bmatrix} \end{aligned} \tag{39}$$

where \ represent the left division symbol in the matrix.

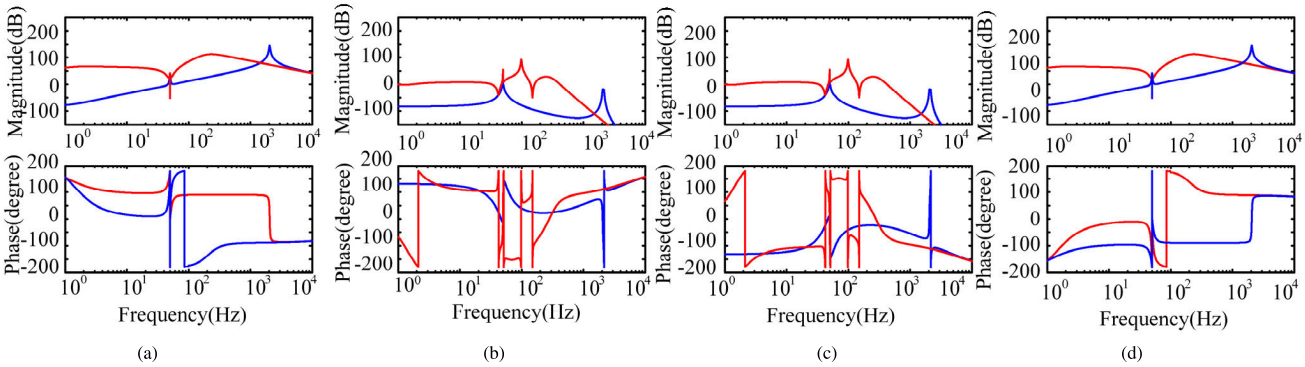

FIGURE 11. Frequency responses of equivalent impedance Z_{eq}: (a) Plots of $Z_{eqss}(s)$; (b) Plots of $Z_{eqsc}(s)$; (c) Plots of $Z_{eqcs}(s)$; (d) plots of $Z_{eqcc}(s)$; Blue line: without harmonic suppression strategy; Red line: with voltage feedback control strategy.

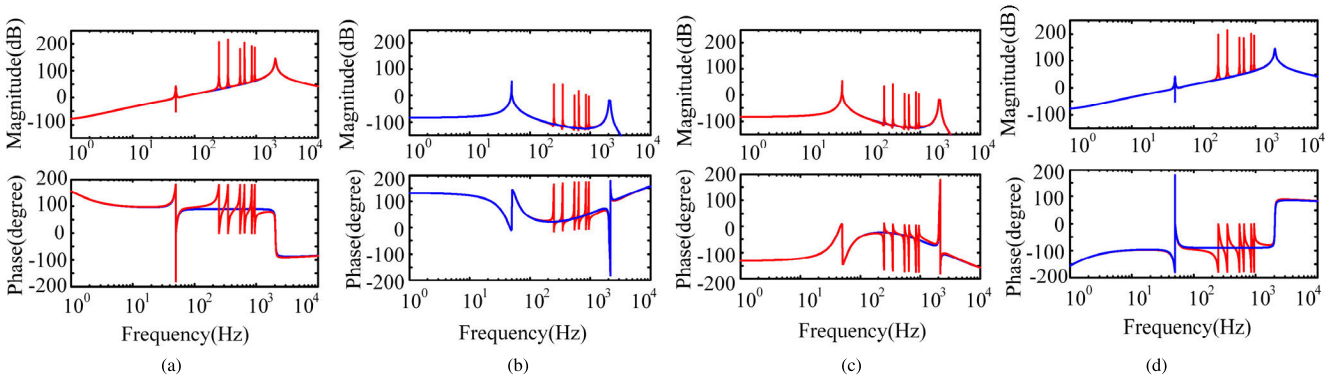

FIGURE 12. Frequency responses of equivalent impedance Z_{eq}: (a) Plots of $Z_{eqss}(s)$; (b) Plots of $Z_{eqsc}(s)$; (c) Plots of $Z_{eqcs}(s)$; (d) plots of $Z_{eqcc}(s)$; Blue line: without harmonic suppression strategy; Red line: with impedance-based harmonic suppression strategy.

The reshaped impedance of the inverter can be expressed as:

$$\mathbf{Z}_{\text{inv}} = \begin{bmatrix} Z_{ss}(s_s) & Z_{sc}(s_c) \\ Z_{cs}(s_s) & Z_{cc}(s_c) \end{bmatrix} \tag{40}$$

On the basis of (17), the series virtual impedance can be expressed as:

$$Z_{\text{vir}}(s) = \frac{K_m V_{\text{dc}} G_{\text{MR}}(s)}{1 + s^2 LC - K_m V_{\text{dc}} G_{mv}(s)} \tag{41}$$

Ignoring the fundamental component and higher-order components, the virtual impedance can be rewritten in the rectangular form of vector expression as:

$$\mathbf{Z}_{\text{vir}} = \left(\begin{bmatrix} 1 + s_s^2 LC & 0 \\ 0 & 1 + s_c^2 LC \end{bmatrix} - K_m V_{\text{dc}} \mathbf{G}_{mv}(s_s - s_1) \right) \backslash K_m V_{\text{dc}} \mathbf{G}_{\text{MR}}(s_s) \tag{42}$$

$$\mathbf{Z}_{\text{g1}} = diag\left(Z_{\text{g1}}(s_s), Z_{\text{g1}}(s_c)\right) \tag{43}$$

In case 1, as seen in Figure 1(b), the equivalent impedance of grid-connected system viewed from PCC to VSG can be derived in the vector expression as:

$$\mathbf{Z}_{\text{eq}} = \mathbf{Z}_{\text{inv}} + \left(\mathbf{Z}_{\text{vir}} + \mathbf{Z}_{\text{g1}}\right) // \mathbf{Z}_{\text{line}} = \begin{bmatrix} Z_{eqss}(s_s) & Z_{eqsc}(s_c) \\ Z_{eqcs}(s_s) & Z_{eqcc}(s_c) \end{bmatrix} \tag{44}$$

In case 2, as seen in Figure 7, the equivalent impedance can be derived in the vector expression as:

$$\mathbf{Z}_{\text{eq}} = \mathbf{Z}_{\text{inv}} + \mathbf{Z}_{\text{vir}} + \mathbf{Z}_{\text{g1}} = \begin{bmatrix} Z_{eqss}(s_s) & Z_{eqsc}(s_c) \\ Z_{eqcs}(s_s) & Z_{eqcc}(s_c) \end{bmatrix} \tag{45}$$

In case 3, as seen in Figure 9, the equivalent impedance can be derived in the vector expression as:

$$\mathbf{Z}_{\text{eq}} = \mathbf{Z}_{\text{inv}} + \left(\mathbf{Z}_{\text{vir}} + \mathbf{Z}_{\text{g1}}\right) // \mathbf{Z}_{\text{line}} = \begin{bmatrix} Z_{eqss}(s_s) & Z_{eqsc}(s_c) \\ Z_{eqcs}(s_s) & Z_{eqcc}(s_c) \end{bmatrix} \tag{46}$$

B. RESHAPING PERFORMANCE ANALYSIS

Figures 11 to 13 show frequency responses of the equivalent impedance Z_{eq} of VSG-based grid-connected system with three different harmonic suppression methods. The parameters of systems are shown in Table 1. The blue lines represent frequency response curves with no harmonic suppression strategy, while the red lines represents frequency response curves with voltage feedback control, strategy impedance-based harmonic suppression strategy, and magnitude-reshaping control strategy, respectively.

Figure 11 shows the frequency response characteristics of VSG with PCC voltage feedback method in red lines. Compare to the results with no harmonic suppression strategy, both the diagonal elements ($Z_{eqss}(s_s)$ and $Z_{eqcc}(s_c)$)

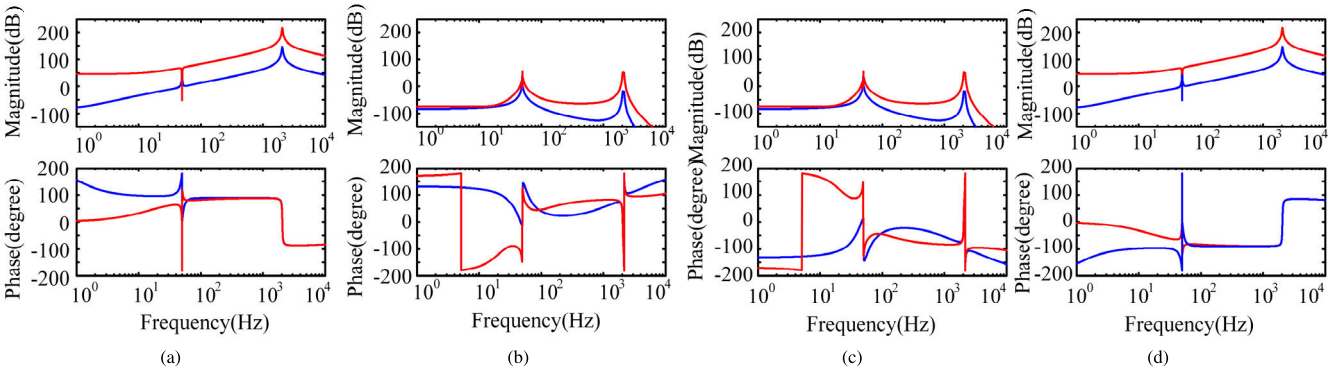

FIGURE 13. Frequency responses of equivalent impedance Z_{eq}: (a) Plots of $Z_{eqss}(s)$; (b) Plots of $Z_{eqsc}(s)$; (c) Plots of $Z_{eqcs}(s)$; (d) plots of $Z_{eqcc}(s)$; Blue line: without harmonic suppression strategy; Red line: with proposed magnitude-reshaping strategy.

TABLE 1. Parameters of grid-connected system.

Parameters	Symbol	Value	Parameters	Symbol	Value
DC-side voltage	V_{dc}	700V	Proportional gain of $K_{PD}(s)$	K_p	10
Grid voltage RMS	v_g	220V	Differential gain of $K_{pr}(s)$	K_d	0.1
Fundamental frequency	f_1	50 Hz	Proportional gain of $G_N(s)$	ω_c	12.56
Switching frequency	f_s	10 Hz	Integrator gain of $G_Q(s)$	K	50
Filter inductor	L	3 mH	Filter capacitor	C	20μF
Rated active power	P_n	20kW	Filter resistance	R_d	10Ω
Rated reactive power	Q_n	0VA	Damper coefficient	D	20
Grid inductor	L_g	2mH	Inertia coefficient	J	0.2
Modulator gain	K_m	350			

and the off-diagonal elements ($Z_{eqsc}(s_c)$ and $Z_{eqcs}(s_s)$) are increased in amplitude significantly in the low-frequency and mid-frequency band, thus the harmonic currents are effectively suppressed. However, the increased off-diagonal elements $Z_{eqsc}(s_c)$ and $Z_{eqcs}(s_s)$ will lead to impedance coupling, which will influence the stability of grid-connected system. According to generalized Nyquist stability criterion, the non-negligible coupled impedance will increase the complexity of stability assessment. Moreover, the reshaping performance of voltage feedback method on high frequency impedance is unsatisfactory.

Figure 12 shows the frequency response characteristics of VSG with impedance-based harmonic suppression strategy in red lines. Because the sampling filter $G_h(s)$ is only designed for the 5th, 7th, 11th, 13th, 17th and 19th harmonic voltages. The equivalent impedance remains unchanged in other frequency bands. The amplitude of the equivalent impedance of the grid-connected system at the above-mentioned special frequency tends to infinity, so it can be guaranteed that these specific harmonics will not exist in the grid-connected currents. As seen, this method cannot suppress non-integer harmonic currents.

Figure 13 shows the frequency response characteristics of VSG with magnitude-reshaping strategy in red lines. In the harmonic frequency the diagonal elements ($Z_{eqss}(s_s)$ and $Z_{eqcc}(s_c)$) significantly increase in magnitude as shown in Figures 8(a) and 8(d), while the impedance response of off-diagonal elements ($Z_{eqsc}(s_c)$ and $Z_{eqcs}(s_s)$) magnitude-reshaping is changed slightly. Therefore, the proposed method will not affect the complexity of the stability assessment of the grid-connected system. Moreover, the magnitude-reshaping method has little effects on the phase-frequency response.

V. EXPERIMENT VALIDATIONS

To validate the proposed method, a HIL experiment platform based on RTLAB and DSP TMS320F28335 is established to verify the effectiveness of the proposed method. The experiment studies three cases as discussed in Section II to compare the performances among the different types of harmonic suppression strategies. Case 1 studies the system with distributed generator connected to PCC, which leads to non-integer-order high-frequency harmonics. Case 2 studies the system with nonlinear load connected to PCC, which leads to integer-order super-synchronous harmonics. Case 3 studies the system with of synchronous generator connected to PCC (with 30Hz sub-synchronous oscillation).

The main circuit parameters and control parameters are shown in Table 1. The control structure of these harmonic suppression methods is shown in Figures 4 and 5, respectively.

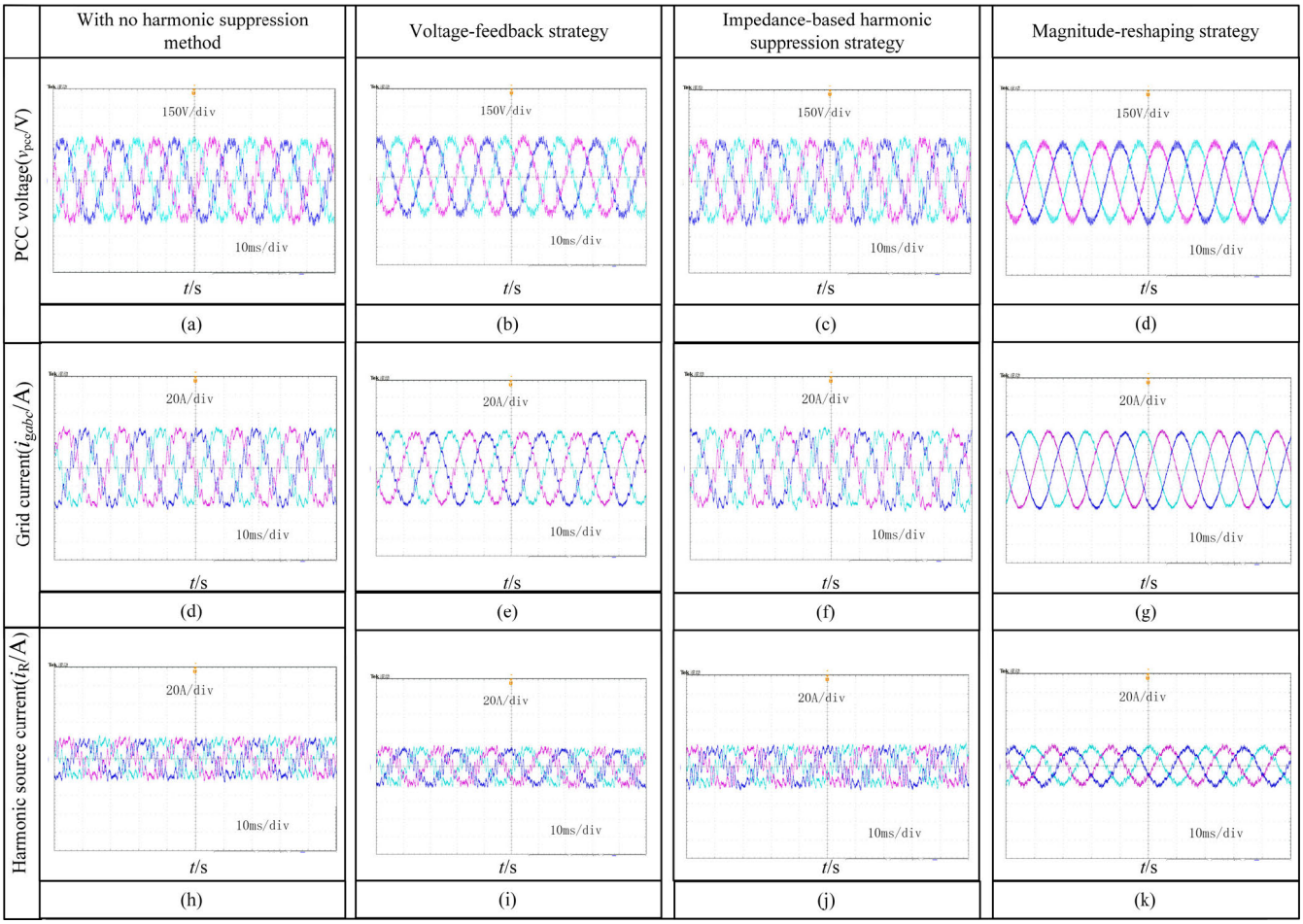

FIGURE 14. Waveforms with different harmonic suppression strategies in Case1.

The VSG controller transfer function is:

$$\begin{cases} G_P(s) = \dfrac{1}{s(0.2s+20)} \\ G_Q(s) = \dfrac{1}{50s} \end{cases} \tag{47}$$

In magnitude-reshaping strategy, the Magnitude-reshaping compensator controller transfer function is:

$$G_{MR}(s) = G_N(s)\,G_{PD}(s) = \frac{s^2+98596}{s^2+25.12s+98596}(10+0.1s) \tag{48}$$

In PCC voltage feedback strategy, the compensator controller transfer function is:

$$G_c(s) = G_N(s)\,K_f = \frac{12\left(s^2+98596\right)}{s^2+25.12s+98596} \tag{49}$$

In impedance-based harmonic suppression method, feedback gain $m = 61$, $n = 60$. And the compensator controller transfer function is:

$$G_h(s) = \sum_{i=5,7,11,13,17,19} \frac{12.56s+\omega_c^2}{s^2+12.56s+(i\omega_n)^2+39.43} \tag{50}$$

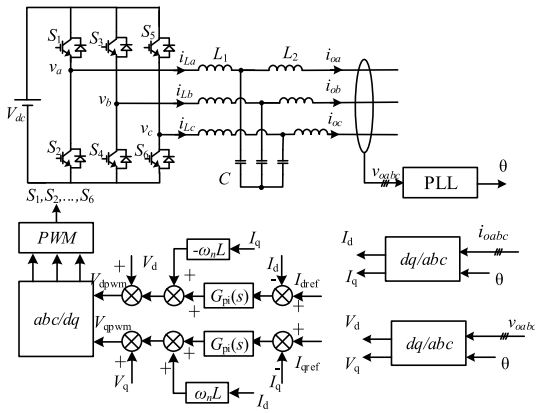

FIGURE 15. Topology of paralleled DG.

Case 1: Topology of VSG in parallel with other current-controlled inverter is shown in Figure 1(a). Figure 14 shows the results of the VSG with three different harmonic suppression methods under case1. The distributed generator is an LCL-based current-controlled inverter with the rated capacity of 20KVA. Impedance of grid line Z_{line} is 1mH. Impedance of

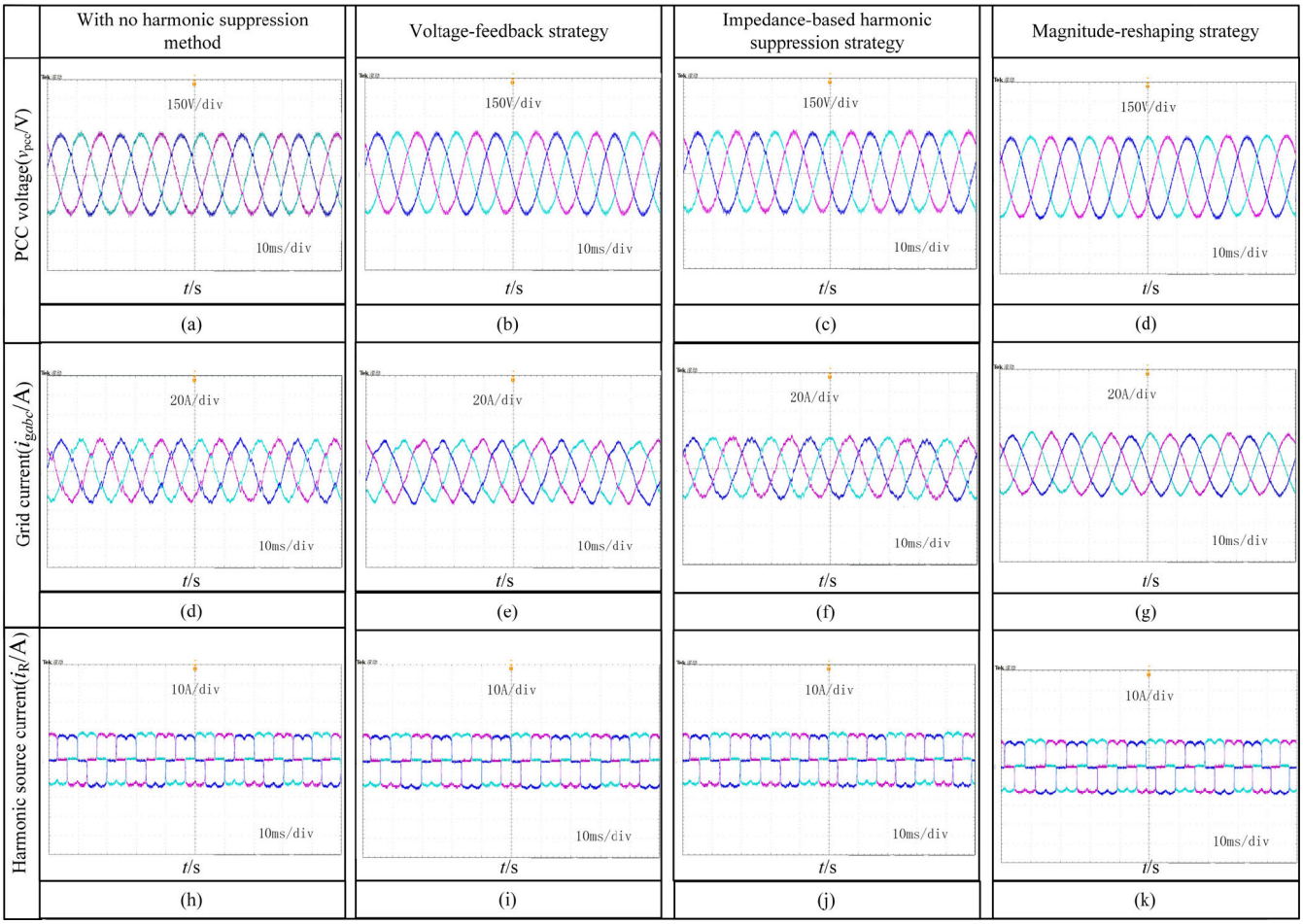

FIGURE 16. Waveforms with different harmonic suppression strategies in Case2.

grid line Z_{g1} is 2mH. The grid impedance Z_{g2} is 6mH. Topology of paralleled DG is shown in Figure 15. The parameters of LCL filter are, $L_1 = 3$mH, $L_2 = 1$mH, and $C = 22\mu$F. The PI controller transfer function in paralleled DG is:

$$G_{\text{pi}}(s) = 0.12 + \frac{340}{s} \tag{51}$$

The PLL transfer function is:

$$T_{\text{PLL}}(s) = \frac{H_{\text{PLL}}(s)}{1 + V_1 H_{\text{PLL}}(s)} \tag{52}$$

where $H_{\text{PLL}}(s) = \left(2.62 + \frac{1650}{s}\right)$.

Due to the grid-source oscillation between distributed generator and the weak grid, i_{R} contains a large amount of non-integer-order harmonic currents, which will affect the PCC voltage v_{pcc} and grid-connected current i_{g}. The interaction oscillations between distributed generation and the grid occurs because of the large grid impedance Z_{g2}.

The waveforms of grid-connected system with no harmonic suppression method are shown in first column of Figure 14. As shown in Figure 14(h), i_{DG} contains a lot of non-integer harmonic components. Affected by i_{DG}, the power quality of PCC voltage and grid current deteriorates in Figures 14(a) and 14(d). The waveforms of the voltage-feedback harmonic suppression method are shown in second column of Figure 14. The control parameter K_f of PCC voltage-feedback method is set to 12. In this case, the THD of the PCC voltage and the grid current decrease. Obviously, voltage-feedback method suppresses the non-integer-order harmonic disturbance. The waveforms of impedance-based harmonic suppression method are shown in third column of Figure 14. Compared with the experimental results without harmonic suppression strategy, the power quality of the power grid is worse. Obviously, impedance-based harmonic suppression method has no harmonic suppression effect on grid-source interaction oscillations. The waveforms of the magnitude-reshaping method are shown in forth column of Figure 14. In the condition, the THD of PCC voltage and grid current decreases sharply. The reason why the power quality of VSG improves is that the differential coefficient K_{d} of the amplitude shaping method makes the output impedance of VSG significantly increase in the high frequency range, so the harmonic path of the grid-connected system is equivalently open circuit. The harmonic current of distributed generator is absorbed by VSG.

Case 2: Figure 16 shows the experiment results with three different types of harmonic suppression methods under

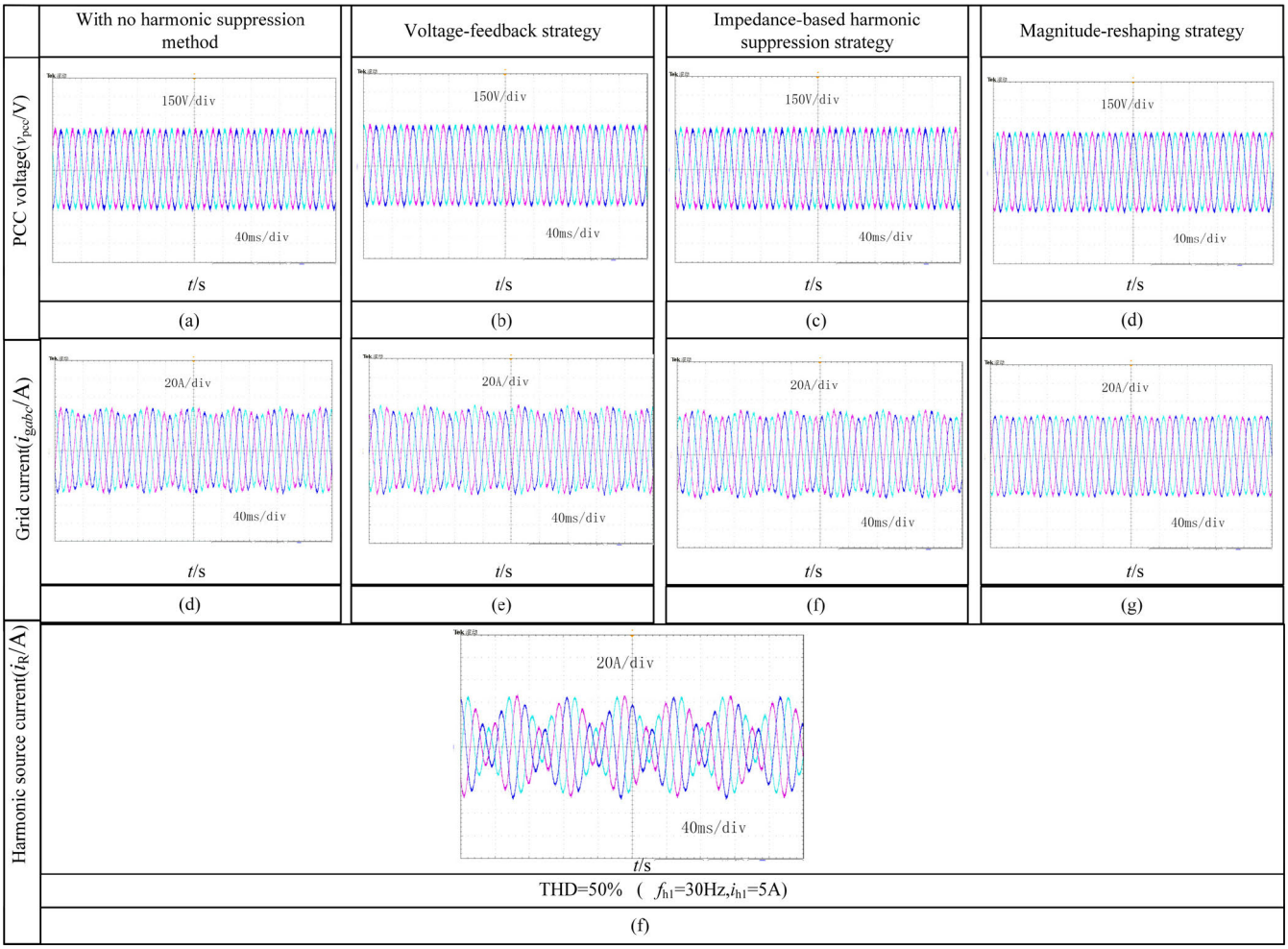

FIGURE 17. **Waveforms with different harmonic suppression strategies in Case3.**

case 2, while the nonlinear load connects to the PCC. Impedance of grid line Z_{g1} is 2mH. The grid impedance Z_{g2} is 6mH. The filter inductor of nonlinear load is 10mH. The rated power of nonlinear load 10KVA.

Due to the switching of diode, the load current in the three phase bridge rectifier circuit, i_R contains a large amount of integer-order harmonic currents, which affects grid-connected power quality.

The waveforms of grid-connected system with no harmonic suppression method are shown in first column of Figure 16. As shown in Figure 16(h), The current of the local nonlinear load is close to a square wave. Affected by i_{DG}, the power quality of PCC voltage and grid current deteriorates as shown in Figures 16(a) and 16(d). The results of the PCC voltage-feedback method are shown in second column of Figure 16. In this case, the THD of the PCC voltage and grid current are reduced, but still contains a small amount of low-order harmonics. The feedback of the PCC voltage makes Z_{eq} increase rapidly in mid-frequency band, so that amplitude of the harmonic gridcurrent reduces. The harmonic suppression effect of the impedance-based method is similar to voltage-feedback method, which are shown in third column of Figure 16. Due to the frequency aliasing effect, i_R contains a small portion of high-frequency harmonics. The waveforms of proposed method are shown in forth column of Figure 16. In this condition, the power quality of PCC voltage and grid current is better than the result of impedance-based harmonic suppression method and PCC voltage-feedback method.

$$\begin{aligned}\mathrm{THD}_{\text{voltage-feedback}} &> \mathrm{THD}_{\text{impedance-based}} \\ &> \mathrm{THD}_{\text{magnitude-reshaping.}}\end{aligned} \tag{53}$$

Since the proportional regulator of magnitude-reshaping method reshapes the output impedance of VSG to a larger value in the mid-frequency band. The harmonic current on the nonlinear load is absorbed by VSG. The power of the nonlinear load determines distortion rate of the PCC voltage. If the power consumed by the non-linear load exceeds the rated capacity of the VSG, the THD of the PCC will increase dramatically. Thus, the magnitude-reshaping strategy is the most effective in solving the PCC voltage distortion caused by nonlinear loads among the three methods.

Case 3: Figure 17 shows the results of the VSG-based grid connected system with three different types of harmonic suppression methods. In this case, the synchronous generator is connected to PCC. In order to imitate the shaft oscillation of the synchronous generator, sub-synchronous currents are injected into the PCC. The power reference of synchronous generator 10KW. The Z_{line} is 1mH. Z_{g1} is 2mH.

The waveforms of grid-connected system with no harmonic suppression method are shown in first column of Figure 17. Both grid-connected current and synchronous motor output current contain obvious sub-synchronous harmonics. It is illustrated that VSG-based grid-connected system has poor robustness against the low-frequency disturbances. The waveforms of the voltage-feedback method are shown in second column of Figure 17. Compared with the results with no harmonics suppression, the THD of the PCC voltage and grid current reduced slightly. The waveforms of impedance-based harmonic suppression method are shown in third column of Figure 17. Since impedance-based harmonic suppression method is aimed at the specified-order harmonics, it is not sensitive to sub-synchronous harmonic disturbances. The waveforms of proposed magnitude-reshaping method are shown in forth column of Figure 17. The harmonic suppression performance is almost the same as the results with voltage-feedforward method. It is illustrated that only magnitude-reshaping method have good performance in low-frequency band.

Based on the above results, it is obvious that voltage feedback method has poor performance at high-frequency band, while impedance-based harmonic suppression method has no suppression effect on low-frequency and high-frequency harmonics. By comparison, the proposed magnitude-reshaping strategy can enhance the robustness of the inverter under weak grids and improve power quality of PCC voltage and grid current in wider frequency ranges, as shown in Table 2.

TABLE 2. Harmonic suppression performance under three cases.

	Case1	Case2	Case3
Voltage-feedback strategy	Effective	Effective	poor
Impedance-based harmonic suppression strategy	poor	Effective	poor
Magnitude-reshaping strategy	Effective	Effective	Effective

VI. CONCLUSION

Conventional harmonic suppression methods for VSG have limited capacity to solve different types of local harmonic problem by one solution. In order to solve this problem, a magnitude-reshaping strategy for suppressing harmonic is proposed in this paper.

Compared with the PCC voltage-feedback method based on notch filter, the proposed method has better robustness to sub-synchronous harmonics. Compared with impedance-based harmonic suppression strategy based on resonant controller, the magnitude-reshaping strategy has better harmonic suppression effects on sub-synchronous harmonics and non-integer-order harmonic. Based on the analysis of the harmonic resonance mechanism, the magnitude-reshaping strategy is designed to increase the equivalent harmonic impedance of VSG-based systems significantly. Therefore, the harmonic currents caused by local harmonic sources can be absorbed by reshaped VSG, and the harmonic components of grid-connected currents decrease sharply. Therefore, the power quality of grid-connected current and PCC voltage can be guaranteed.

Another contribution of this paper is the establishment of the frequency-coupling impedance model of the VSG-based grid-connected system. The model intuitively reflects the performance of impedance reshaping. The frequency response of the coupling impedance shows that in the above three methods, only magnitude-reshaping strategy has the least influence on the off-diagonal elements in impedance matrix. Therefore, this method has the least impact on the grid-connected stability assessment.

In general, the magnitude-reshaping method is proved to be an efficient solution for weak grid with harmonic sources.

REFERENCES

[1] J. Fang, R. Zhang, H. Li, and Y. Tang, "Frequency derivative-based inertia enhancement by grid-connected power converters with a frequency-locked-loop," *IEEE Trans. Smart Grid*, vol. 10, no. 5, pp. 4918–4927, Sep. 2019.

[2] H. Liu and J. Sun, "Voltage stability and control of offshore wind farms with AC collection and HVDC transmission," *IEEE J. Emerg. Sel. Topics Power Electron.*, vol. 2, no. 4, pp. 1181–1189, Dec. 2014.

[3] W. Yang and M. Wang, "Impedance modeling and output impedance coupling analysis of three-phase grid-connected inverters," in *Proc. IEEE Int. Power Electron. Appl. Conf. Exposit. (PEAC)*, Nov. 2018, pp. 1–5.

[4] Q.-C. Zhong and G. Weiss, "Synchronverters: Inverters that mimic synchronous generators," *IEEE Trans. Ind. Electron.*, vol. 58, no. 4, pp. 1259–1267, Apr. 2011.

[5] J. Sun, M. Li, Z. Zhang, T. Xu, J. He, H. Wang, and G. Li, "Renewable energy transmission by HVDC across the continent: System challenges and opportunities," *CSEE J. Power Energy Syst.*, vol. 3, no. 4, pp. 1–11, Dec. 2017.

[6] Y. Song and F. Blaabjerg, "Overview of DFIG-based wind power system resonances under weak networks," *IEEE Trans. Power Electron.*, vol. 32, no. 6, pp. 4370–4394, Jun. 2017.

[7] J. Sun, "Impedance-based stability criterion for grid-connected inverters," *IEEE Trans. Power Electron.*, vol. 26, no. 11, pp. 3075–3078, Nov. 2011.

[8] R. N. Beres, X. Wang, F. Blaabjerg, M. Liserre, and C. L. Bak, "Optimal design of high-order passive-damped filters for grid-connected applications," *IEEE Trans. Power Electron.*, vol. 31, no. 3, pp. 2083–2098, Mar. 2016.

[9] L. Harnefors, X. Wang, A. G. Yepes, and F. Blaabjerg, "Passivity-based stability assessment of grid-connected VSCs—An overview," *IEEE J. Emerg. Sel. Topics Power Electron.*, vol. 4, no. 1, pp. 116–125, Mar. 2016.

[10] D. Pan, X. Ruan, C. Bao, W. Li, and X. Wang, "Optimized controller design for *LCL*-type grid-connected inverter to achieve high robustness against grid-impedance variation," *IEEE Trans. Ind. Electron.*, vol. 62, no. 3, pp. 1537–1547, Mar. 2015.

[11] X. Wang, X. F. Blaabjerg, and P. C. Loh, "Grid-current-feedback active damping for LCL resonance in grid-connected voltage source inverters," *IEEE Trans. Power Electron.*, vol. 3, no. 1, pp. 213–223, Mar. 2016.

[12] D. Pan, X. Ruan, C. Bao, W. Li, and X. Wang, "Capacitor-current-feedback active damping with reduced computation delay for improving robustness of LCL-type grid-connected inverter," *IEEE Trans. Power Electron.*, vol. 29, no. 7, pp. 3414–3427, Jul. 2014.

[13] J. He, Y. W. Li, D. Bosnjak, and B. Harris, "Investigation and active damping of multiple resonances in a parallel-inverter-based microgrid," *IEEE Trans. Power Electron.*, vol. 28, no. 1, pp. 234–246, Jan. 2013.

[14] X. Chen, X. Ruan, D. Yang, W. Zhao, and L. Jia, "Injected grid current quality improvement for a voltage-controlled grid-connected inverter," *IEEE Trans. Power Electron.*, vol. 33, no. 2, pp. 1247–1258, Feb. 2018.

[15] X. Li, J. Fang, Y. Tang, X. Wu, and Y. Geng, "Capacitor-voltage feedforward with full delay compensation to improve weak grids adaptability of LCL-filtered grid-connected converters for distributed generation systems," *IEEE Trans. Power Electron.*, vol. 33, no. 1, pp. 749–764, Jan. 2018.

[16] Z. Xin, P. C. Loh, X. Wang, F. Blaabjerg, and Y. Tang, "Highly accurate derivatives for LCL-filtered grid converter with capacitor voltage active damping," *IEEE Trans. Power Electron.*, vol. 31, no. 5, pp. 3612–3625, May 2016.

[17] L. Zhou, Z. Shuai, Y. Chen, W. Wu, X. Zhou, K. Yan, and A. Luo, "Impedance-based harmonic current suppression method for VSG connected to distorted grid," *IEEE Trans. Ind. Electron.*, vol. 67, no. 7, pp. 5490–5502, Jul. 2020.

[18] X. Ruan, W. Zhao, Z. Lin, and X. Wang, "An adaptive active damper for improving the stability of grid-connected inverters under weak grid," *IEEE Trans. Power Electron.*, vol. 33, no. 11, pp. 9561–9574, Jan. 2018.

[19] Y. A.-R.-I. Mohamed, "Suppression of Low- and high-frequency instabilities and grid-induced disturbances in distributed generation inverters," *IEEE Trans. Power Electron.*, vol. 26, no. 12, pp. 3790–3803, Dec. 2011.

[20] J. Xu, S. Xie, and T. Tang, "Improved control strategy with grid-voltage feedforward for LCL-filter-based inverter connected to weak grid," *IET Power Electron.*, vol. 7, no. 10, pp. 2660–2671, Oct. 2014.

[21] M. Liserre, A. Dell'Aquilla, and F. Blaabjerg, "Genetic algorithm based design of the active damping for a LCL-filter three-phase active rectifier," *IEEE Trans. Power Electron.*, vol. 19, no. 1, pp. 234–240, Jan. 2003.

[22] J. Dannehl, M. Liserre, and F. W. Fuchs, "Filter-based active damping of voltage source converters with *LCL* filter," *IEEE Trans. Ind. Electron.*, vol. 58, no. 8, pp. 3623–3633, Aug. 2011.

[23] R. P. Alzola, M. Liserre, F. Blaabjerg, M. Ordonez, and T. Kerekes, "A self-commissioning notch filter for active damping in a threephase LCL-filter-based grid-tie converter," *IEEE Trans. Power Electron.*, vol. 29, no. 12, pp. 6754–6761, Dec. 2014.

[24] S. Zhang, S. Jiang, X. Lu, B. Ge, and F. Z. Peng, "Resonance issues and damping techniques for grid-connected inverters with long transmission cable," *IEEE Trans. Power Electron.*, vol. 29, no. 1, pp. 110–120, Jan. 2014.

[25] N. A. Rufa'I, L. Zhang, and B. Chong, "Performance analysis of adaptive notch filter active damping methods for grid-connected converters under a varying grid impedance," in *Proc. IEEE Manchester PowerTech*, Jun. 2017, pp. 1–6.

[26] A. Asrari, M. Mustafa, M. Ansari, and J. Khazaei, "Impedance analysis of virtual synchronous generator-based vector controlled converters for weak AC grid integration," *IEEE Trans. Sustain. Energy*, vol. 10, no. 3, pp. 1481–1490, Jul. 2019.

[27] H. Wu, X. Ruan, D. Yang, X. Chen, W. Zhao, Z. Lv, and Q.-C. Zhong, "Small-signal modeling and parameters design for virtual synchronous generators," *IEEE Trans. Ind. Electron.*, vol. 63, no. 7, pp. 4292–4303, Jul. 2016.

[28] C. Hu, K. Chen, S. Luo, B. Zhou, and L. Ding, "Small signal modeling and stability analysis of virtual synchronous generators," in *Proc. 20th Int. Conf. Electr. Mach. Syst. (ICEMS)*, Aug. 2017, pp. 1–5.

[29] X. Xie, X. Zhang, H. Liu, H. Liu, Y. Li, and C. Zhang, "Characteristic analysis of subsynchronous resonance in practical wind farms connected to series-compensated transmissions," *IEEE Trans. Energy Convers.*, vol. 32, no. 3, pp. 1117–1126, Sep. 2017.

[30] W. Wu, M. Zhang, Y. Chen, L. Zhou, A. Luo, X. Zhou, Z. He, L. Yang, Z. Xie, and J. Liu, "Sequence impedance modeling and stability comparative analysis of voltage-controlled VSGs and current-controlled VSGs," *IEEE Trans. Ind. Electron.*, vol. 66, no. 8, pp. 6460–6472, Aug. 2019.

[31] X. Wang, L. Harnefors, and F. Blaabjerg, "Unified impedance model of grid-connected voltage-source converters," *IEEE Trans. Power Electron.*, vol. 33, no. 2, pp. 1775–1787, Feb. 2018.

[32] W. Liu, Z. Lu, X. Wang, and X. Xie, "Frequency-coupled admittance modelling of grid-connected voltage source converters for the stability evaluation of subsynchronous interaction," *IET Renew. Power Gener.*, vol. 13, no. 2, pp. 285–295, Feb. 2019.

[33] X. Wang, L. Harnefors, F. Blaabjerg, and P. C. Loh, "A unified impedance model of voltage-source converters with phase-locked loop effect," in *Proc. IEEE Energy Convers. Congr. Expo. (ECCE)*, Sep. 2016, pp. 1–8.

WEN YANG was born in 1992. He received the B.Eng. degree in electrical engineering from Chongqing University, Chongqing, China, in 2014, where he is currently pursuing the Ph.D. degree in electrical engineering. His research interests include modeling and control of power electronics converters, renewable energy generation, and stability analysis.

MINGYU WANG was born in 1960. He received the B.Eng. degree in electrical engineering from Chongqing University, China, in 1982, and the Ph.D. degree from Liverpool John Moores University, U.K., in 1999. He became a member of the Academic Staff, Department of Automation Engineering, Chongqing University, in 1982, where he was a Lecturer, from 1988 to 1993. He was a Visiting Scholar with the Department of Electrical Engineering, The University of Manchester, U.K., from 1993 to 1995. He is currently a Professor with Chongqing University. His research interests include power converters, power filters, adjustable speed drives, and vector control of induction machines.

SADDAM AZIZ (Member, IEEE) received the Ph.D. degree in optoelectronics engineering from Shenzhen University, Shenzhen, China, in 2019, and the M.Eng. degree in electrical engineering from Chongqing University, Chongqing, China, in 2015. He was a Visiting Professor with the China University Summer Schools Association, China, from 2018 to 2020. He is currently a Research Associate Professor with the College of Mechatronics and Control Engineering, Shenzhen University, Shenzhen. He was declared as a Professional Electrical Engineer by Engineers Australia, in 2017. His research interests include cyber physical power systems, artificial intelligence, renewable energy integration, and mainly multi-terminal HVDC multi-terminal dc system operation, optimization, and planning.

ALI YOUSAF KHARAL (Member, IEEE) received the M.S. degree in electrical engineering power from NUST, Islamabad, Pakistan. He is currently an Electrical Engineer. His research interests include smart grid, power electronics, and applications of machine learning to power systems.